Thermal proteome profiling identifies oxidative-dependent inhibition of the transcription of major oncogenes as a new therapeutic mechanism for select anticancer compounds

Sylvain Peuget[1,*], Jiawei Zhu[1], Gema Sanz[1], Madhurendra Singh[1], Massimiliano Gaetani[2,3], Xinsong Chen[4], Yao Shi[1], Amir Ata Saei[2], Torkild Visnes[3,4,5], Mikael S. Lindström[2,3], Ali Rihani[1], Lidia Moyano-Galceran[1], Joseph W. Carlson[4], Elisabet Hjerpe[4], Ulrika Joneborg[6], Kaisa Lehti[1], Johan Hartman[4], Thomas Helleday[3,4,7], Roman Zubarev[2,3], Galina Selivanova[1,*]

[1] Department of Microbiology, Tumor and Cell Biology, Karolinska Institutet, Stockholm, Sweden

[2] Department of Medical Biochemistry and Biophysics, Karolinska Institutet, Stockholm, Sweden

[3] Science for Life Laboratory, Stockholm, Sweden

[4] Department of Oncology-Pathology, Karolinska Institutet, Karolinska University Hospital, Stockholm, Sweden

[5] Department of Biotechnology and Nanomedicine, SINTEF Industry, Trondheim, Norway

[6] Division of Obstetrics and Gynecology, Department of Women's and Children's Health, Karolinska Institutet, Karolinska University Hospital, Stockholm, Sweden

[7] Weston Park Cancer Centre, Department of Oncology and Metabolism, University of Sheffield, Sheffield, UK

[*] Corresponding authors: S Peuget, sylvain.peuget@ki.se; Department of Microbiology, Tumor and Cell Biology, Karolinska Institutet, 171 77 Stockholm; Sweden; Tel: +46 8 52486273. G Selivanova, galina.selivanova@ki.se; Department of Microbiology, Tumor and Cell Biology, Karolinska Institutet, 171 77 Stockholm; Sweden; Tel: +46 8 52486302.

Running title: TPP reveals the mechanism of selective anticancer compounds

Keywords: RITA, Aminoflavone, Oncrasin, RNA processing, Thermal proteome profiling

Conflicts of interests

The authors declare no potential conflicts of interest.

ABSTRACT

Identification of the molecular mechanism of action (MoA) of bioactive compounds is a crucial step for drug development but remains a challenging task despite recent advances in technology. In this study, we applied multidimensional proteomics, sensitivity correlation analysis and transcriptomics to identify a common mechanism of action for the anticancer compounds RITA, aminoflavone (AF) and oncrasin-1 (Onc-1). Global thermal proteome profiling (TPP) revealed that the three compounds target mRNA processing and transcription, thereby attacking a cancer vulnerability - transcriptional addiction. This led to the preferential loss of expression of oncogenes involved in PDGF-, EGFR-, VEGF-, Insulin/IGF/MAPKK-, FGF-, Hedgehog-, TGF-beta- and PI3K-signaling pathways. Increased reactive oxygen species (ROS) level in cancer cells was a prerequisite for targeting the mRNA transcription machinery, thus conferring cancer-selectivity to these compounds. Furthermore, DNA repair factors involved in homologous recombination were among the most prominently repressed proteins. In cancer patient samples, RITA, AF and Onc-1 sensitized to poly(ADP-ribose) polymerase inhibitors both *in vitro* and *ex vivo*. These findings might pave a way for new synthetic lethal combination therapies.

Significance

Findings highlight agents that target transcriptional addiction in cancer cells and suggest combination treatments that target RNA processing and DNA repair pathways simultaneously as effective cancer therapies.

INTRODUCTION

Comprehensive assessment of MoA and drug-protein interactions in living cells constitutes a major challenge for rationalizing a drug's therapeutic and adverse effects. Multiple strategies for target deconvolution have been developed, but many of them include compound modification/labeling (1). Recently developed TPP enables such an assessment in a physiologically relevant cellular environment without compound modification and at a proteome-wide level. TPP is based on the principle that the heat-induced unfolding of proteins changes upon binding to ligand. Using quantitative mass spectrometry-based proteomics, TPP measures ligand-induced thermal stabilization or destabilization of proteins (2). The changes in melting proteome reflect direct drug-protein binding but also the changes in post-translational modifications and protein-protein interactions. Therefore, the shift in thermal stability of proteins could be used not only for the prediction of direct drug targets, but also for an unbiased identification of molecular MoA.

Cancer cells are subject to multiple stresses, including genotoxic, proteotoxic, replicative, metabolic and oxidative stresses. Tumor cells adapt to detrimental stressful conditions by dysregulated gene expression. This creates a dependence on continuous active transcription of oncogenes (3). Transcriptional addiction emerged as a potential ‘Achilles’ heel’ of cancer cells that can be therapeutically exploited. However, targeting transcription for selective elimination of cancer cells has been considered difficult due to potential toxicity for normal tissues. The development of CDK7 and CDK12/13 inhibitors have challenged this paradigm: although acting on numerous genes, they exert a highly specific effects on gene expression (3). These compounds selectively affect cancer cells, leading to a preferential loss of oncogenic gene expression, along with DNA damage response genes (4). Attacking addiction to a single oncogene is the basis of targeted therapies (5), but invariably leads to emergence of resistance clones due to cancer cells’ plasticity. Therefore, targeting addiction to multiple oncogenes, either with a single compound or combinatorial treatments, is an attractive anti-cancer strategy to limit acquired resistance.

In this study, we applied multidimensional approaches, including TPP, to identify the MoA and pathways affected by selective anticancer compounds RITA, AF and Onc-1 and investigated how these new findings might provide opportunities for novel combination therapies.

MATERIALS AND METHODS

Cell lines

MCF7, T47D, A375, U2OS, OVCAR-3, 184A1, MCF10A and BJ-hTERT were obtained from ATCC. BJ-hTert HRasV12$^{ER\text{-}Tam}$ cells were a kind gift from Reuven Agami, Netherland. U2OS cMyc$^{ER\text{-}Tam}$ cells were obtained from Martin Eilers, Germany. CRISPR/Cas9 mediated p53 deletion was performed in MCF7 and A375 cells using sgRNA targeting TP53 exon 4. Cell lines were authenticated by ATCC and mycoplasma contamination was tested monthly using MycoAlert Mycoplasma detection kit (Lonza) according to supplier instructions. All experiments were performed within 20 passages from frozen stocks. Further details can be found in Supplementary Materials and Methods and Supplementary Table S1.

Clinical samples

Experiments on primary cancer cells from breast cancer patients and ascites fluid from patients with metastatic HGS-OC were approved by the Regional Ethical Board of Stockholm (Dnr 2016/957-31, 2017/742-32 and 2016/1197-31/1) in compliance with the declaration of Helsinki. Samples were taken from patients who signed written informed consent. Detailed information about isolation procedure and treatments can be found in Supplementary Materials and Methods.

Compounds and treatments

RITA (NSC652287) and aminoflavone (NSC686288) were obtained from the National Cancer Institute (NCI), while oncrasin-1 was from Santa Cruz Biotechnology. Unless stated otherwise, cells were treated in complete medium with 1 μM RITA, 1 μM AF or 5 μM Onc-1. α-amanitin, ActD, BMH21, camptothecin, cycloheximide, irinotecan, MG132, NDGA, Nutlin-3 and resveratrol were purchased from Sigma-Aldrich; cisplatin, doxorubicin, olaparib and talazoparib from Selleckchem; THZ531 from ApexBio Technology. For combination experiment with PARP inhibitors, cells were pretreated 2 days with olaparib or talazoparib and then treated with the combination for the indicated time.

Antibodies

All antibodies used in the study are detailed in Supplementary Materials and Methods.

qPCR

Total RNA extraction and cDNA synthesis were performed using Aurum total RNA and iScript cDNA synthesis kits (Bio-Rad) according to supplier instructions. mRNA quantification was performed by RT-qPCR using Sso Advanced Universal SYBRGreen SuperMix (Bio-Rad). GAPDH and RPL13A were used as housekeeping genes. Error bars represent standard deviation from mean of at least three independent experiments. The sequences of qPCR primers used are detailed in Supplementary Table S2.

Correlation sensitivity analysis

NCI-60 analysis tools provided by CellMiner (https://discover.nci.nih.gov/cellminer/)(6) and the NCI-60 cell line panel with associated drug screens were used to calculate the drug sensitivity Pearson correlation coefficient between RITA, AF and Onc-1, as well as the correlation between RITA, DNA-damaging agents and topoisomerase-1 (TOP1) inhibitors. The 50% growth inhibitory concentration (GI50) values of drugs were used for calculations.

Thermal proteome profiling

MCF7 cells were treated with 1 μM RITA, 1 μM AF or 5 μM Onc-1 for 2h (RITA and AF) or 6h (Onc-1) in biological duplicates. TPP was performed as previously described (7). Briefly, cells from each biological replicate were split equally into ten parts; each aliquot was heated at a different temperature point ranging from 37°C to 67°C. Soluble proteins were then analyzed by quantitative LC-MS/MS. For each protein, the melting temperature (Tm) was calculated and proteins with $|\Delta Tm| \geq 0.5°C$ and *p*-value <0.05 were considered as hits for subsequent analyses. Sample processing and data analysis are detailed in Supplementary Materials and Methods, and the complete list of TPP hits for each compound treatment in MCF7 cells can be found in Supplementary Table S3.

GO statistical overrepresentation analysis was performed using PANTHER (Protein ANalysis THrough Evolutionary Relationships 13.1 (http://pantherdb.org)(8) against all human genes. PANTHER GO-Slim biological processes enriched in TPP hits with Fisher adjusted *p*-value < 0.01 were considered as affected by each treatment. The complete list of GO-Slim biological processes enriched in TPP hits can be found in Supplementary Table S4. Functional protein interaction network analysis was performed using STRING 10.5 (http://string-db.org)(9). The STRING network was built with all proteins affected by at least one treatment. Only interactions with the highest score (>0.900) from experiments or curated databases were considered. The 3 main clusters of the network were identified by k-mean clustering, and each cluster was analyzed for GO statistical overrepresentation using PANTHER to identify its biological function.

Microarrays

Expression profiling of MCF7 cells treated with 1 µM RITA, 10 µM Nutlin (8h), or with 1 µM AF (8h), 5 µM Onc-1 (16h) was performed using GeneChip HG-U219 or HT HG-U133+ PM 24-Array Plate respectively. The datasets generated in the current study are available in GEO database (https://www.ncbi.nlm.nih.gov/geo/) under accession number GSE86880 and GSE128329, and in Supplementary Table S5. Data analysis is detailed in Supplementary Materials and Methods.

Cell viability assays

Cell viability was assessed by resazurin assay. Briefly, cells were treated for 24h to 72h and incubated 2h with 5 µM resazurin (Sigma-Aldrich) before fluorescence measurement on a VICTOR X5 plate reader (PerkinElmer). For crystal violet staining experiments, cells were treated for 1 to 5 days, fixed with ethanol and stained with 0.2% crystal violet. Quantification was performed using ImageJ software.

ROS measurement

Cells were treated as indicated for 8h, then washed and incubated 30 min with 10 μM DCFDA in serum free medium. Then cells were trypsinized, washed twice with PBS and fluorescence was analyzed by a FACSCalibur flow cytometer (BD Biosciences).

EU labelling

Cells on glass coverslips were treated for the indicated time, and 1 mM EU was added to the medium 1h before cell fixation. EU was labelled using the Click-iT RNA Alexa Fluor 594 Imaging Kit (Thermo Fisher Scientific) according to the manufacturer's instructions.

HR reporter assay

HR reporter assay was performed in U2OS cells harboring stably integrated reporter construct for HR (DR-GFP) as described (10). To generate a DSB, U2OS DR-GFP cells were transfected with I-SceI expression vector pCMV3xnls-I-SceI (1 μg) using Fugene HD (Promega). 24h after transfection, cells were treated with RITA, AF or Onc-1 for 16h and GFP fluorescence due to homologous recombination of I-SceI cleavage site was monitored by flow cytometry.

Statistics

Unless otherwise stated, statistical significance was calculated using two-tailed Student's *t*-test.

RESULTS

Similarity of phenotypes induced in cancer cells by RITA, AF and Onc-1

RITA (Reactivation of p53 and induction of tumor cells apoptosis) was identified by us in a screen for molecules that selectively kill cells expressing wild type (wt) p53. RITA is a potent anti-cancer agent *in vitro* and *in vivo* and is highly selective for cancer, but not normal cells (11,12). Using several pairs of isogenic cancer cells with wtp53/KOp53, we found that the contribution of p53 to cell death upon RITA is cell type-dependent (**Supplementary Fig. S1A-J**). While in melanoma A375 cells RITA effects were completely p53-dependent (**Supplementary Fig. S1I-J**), in MCF7 cells the contribution of p53 to the effects of RITA was quite weak, although detectable (**Supplementary Fig. S1A-H**), in line with recently published data (13).

To address the p53-independent MoA of RITA, we took advantage of ProTargetMiner database, containing proteome profiles for 56 anti-cancer drugs in A549 lung cancer cells (14). Since protein abundances depend not only on mRNA levels, but also on translation rate and protein stability, proteome response can be highly specific to drug MoA. We compared the proteome signature upon RITA treatment to 20 other anticancer compounds. Unsupervised clustering revealed the similarity of RITA and anti-metabolic drugs raltitrexed and methotrexate profiles (**Fig. 1A**). However, RITA profile did not cluster with DNA damaging compounds such as bleomycin or doxorubicin, suggesting that its MoA is different from that of DNA damaging drugs.

Next, we searched the NCI-60 cancer cell lines pharmacology database for compounds eliciting a sensitivity profile similar to RITA. Consistent with our chemical proteomics analysis, RITA sensitivity profile did not correlate with those of DNA damaging drugs (such as cisplatin, oxaliplatin), topoisomerase inhibitors (camptothecin, irinotecan, topotecan) or ROS-inducing compounds (doxorubicin) (**Supplementary Fig. S2A**). We also compared transcriptional changes induced by RITA treatment with those upon cisplatin, doxorubicin, camptothecin, irinotecan or Nutlin-3 in MCF7 cells (**Supplementary**

Fig. S2B). While the response of p53-activated genes PUMA, NOXA and p21 was similar, the repression of oncogenes MDM2, PPM1D and MCL1 occurred only upon RITA treatment. These results were confirmed at protein level (**Supplementary Fig. S2C**). Further, comparison of genome-wide expression upon RITA, Nutlin-3, camptothecin, cisplatin and doxorubicin revealed a very distinct transcriptional profile upon RITA treatment (**Supplementary Fig. S2D**). Taken together, our analysis of proteomics, transcriptomics and cancer cell sensitivity profiles upon RITA revealed a response different from that induced by DNA damaging compounds, ROS inducers or topoisomerase inhibitors.

Notably, sensitivity correlation analysis of NCI-60 database revealed a significant correlation between the sensitivity of cancer cells to RITA and the two anticancer compounds AF and Onc-1 (R^2=0.5938 and R^2=0.6466, respectively) (**Fig. 1B-C**).

AF (5-amino-2-(4-amino-3-fluorophenyl)-6,8-difluoro-7-methylchromen-4-one; NSC 686288) displays an anti-proliferative and pro-apoptotic activity in tumor cells (15). It induces replication-dependent DNA lesions and S-phase dependent apoptosis (16), although its MoA has not been fully elucidated. Onc-1 (1-[(4-chlorophenyl)methyl]-1H-indole-3-carboxaldehyde) and its derivative NSC-743380, identified in a screen for selective targeting of mutant K-Ras cancer cells (17), exhibit antitumor activity in several tumors types (18). Onc-1 MoA remains unclear, but involves interference with RNA polymerase II (RNA pol II) transcription and STAT3 inhibition (19,20).

Cancer selectivity is crucial for the success of anti-cancer compounds. Therefore, we compared the effect of these compounds on the growth of normal and cancer cells (**Fig. 1D**). RITA, AF and Onc-1 efficiently reduced cell viability in breast cancer cells MCF7 and T47D, whereas they had a limited effect on normal mammary epithelial cells 184A1 and MCF10A and non-transformed BJ-hTert fibroblasts.

Furthermore, we found that the treatment of MCF7 cells with AF or Onc-1 phenocopied RITA effects on apoptosis and DNA damage response, although the kinetics was slightly different for Onc-1 (**Fig. 1E** and **Supplementary Fig. S3A**). The three compounds activated the c-Jun N-terminal kinase (JNK) pathway

(**Fig 1E**), in line with previous studies (19,21,22). We found previously that RITA inhibits the antioxidant enzyme thioredoxin reductase 1 (TrxR1) (23), increasing intracellular ROS level. Similarly, AF and Onc-1 induced a strong oxidative stress in different cell lines (**Fig 1F** and **Supplementary Fig. S3B**).

Since growth suppression by RITA depends on the downregulation of several crucial oncogenes (12,22), we tested whether AF and Onc-1 have similar effects. Indeed, MDM2, PPM1D, MCL1 and MDMX were inhibited on mRNA and protein level upon treatment with all three compounds, along with the induction of pro-apoptotic PUMA and NOXA (**Fig. 2A-B** and **Supplementary Fig. S3C**). Interestingly, while p21 mRNA was induced, its protein level was downregulated by AF and Onc-1, similar to the effects we have shown previously for RITA (24). Finally, as RITA, AF and Onc-1 all stabilize p53 in MCF7 cells (**Fi.g 1E**), we performed viability assays in p53 KO MCF7 and showed that apoptosis caused by all three compounds was largely p53-independent in these cells (**Supplementary Fig. S3D**).

Furthermore, we observed a remarkably similar expression profile upon RITA, AF and Onc-1, and identified 3154 common differentially expressed genes (DEGs) in MCF7 cells (**Fig. 2C-D**). Strikingly, oncogenes were overrepresented among common repressed genes (**Fig. 2E**). Analysis of gene expression data revealed significant downregulation of oncogenes representing major oncogenic pathways, such as PDGF-, EGFR-, VEGF-, Insulin/IGF/MAPKK-, FGF-, Hedgehog-, TGF-beta- and PI3K-signaling pathways (**Fig. 2F-G and Supplementary Fig. S3E**).

TPP identifies RNA processing as the common cell process affected by RITA, AF and Onc-1

Since RITA, AF and Onc-1 induced a highly similar cell response, we hypothesized that they could have a common molecular target, and/or target a common pathway. To identify pathways affected by the three compounds, we performed TPP in MCF7 cells. Identifying a direct drug target with TPP is challenging, as many variations in protein interactions measured in the cells could be secondary, indirect events. Instead, the proteome-wide variations in protein interactions provide important clues as to which pathways are

affected by a drug. Therefore, we considered the changes of interactions observed upon treatment as a reflection of the key affected biological processes.

To minimize the indirect events, we analyzed proteome changes at early time points (2h for RITA and AF, 6h for Onc-1). We identified 144, 182 and 188 hits, defined as proteins with a significant thermal shift $|\Delta Tm| \geq 0.5°C$ upon treatment with RITA, Onc-1 and AF, respectively (**Fig. 3A-B**), with a prominent overlap among them (**Fig. 3B** and **Supplementary Fig. S4A**). We identified 90 hits common for two treatments and 8 hits common for all three treatments. We performed a Gene Ontology (GO) analysis using PANTHER to identify biological processes affected (**Fig. 3C**). Notably, most of the GO biological processes terms enriched in TPP hits were related to RNA processing, including splicing and RNA metabolism. The overlap between the GO biological processes terms was striking, with RNA processing being the common process affected by all three treatments (**Fig. 3D**). Mitochondrial translation was also significantly affected upon AF treatment, but not upon RITA and Onc-1.

As TPP detects the changes of interactions for a given protein, other proteins interacting with a TPP hit are likely to be also affected. In order to have a more integrated view of the changes in protein complexes involved, we generated a protein-protein interaction network using STRING to visualize the functional interactions affected by RITA, AF and Onc-1 (**Fig. 3E** and **Supplementary Fig. S4B**). Using unbiased K-means clustering, we identified three main clusters of interactions in the network (clusters A, B and C), containing 34, 20 and 16 proteins, respectively. The proportion of proteins in the clusters affected by each treatment is shown in **Figure 3F**. To identify the biological function of each cluster, we performed a GO analysis (**Fig. 3G**). Cluster A represents proteins involved in RNA processing, including multiple splicing factors and auxiliary splicing regulatory proteins (MAGOH, RBM8A, DHX38, SF1, SF3B1, SF3B2, SF3B4, RBM22, SUGP1, PTPB1, HNRNPM, SNRPC), RNA polymerase II subunits (POLR2A, POR2L, POLR2K), transcriptional elongation regulators (RDBP) and polyadenylation factors (CPSF1, CSTF1, PAPOLA). Importantly, this cluster was affected evenly by the three treatments. Cluster C has a less

defined biological function, including proteasome subunits, cell cycle regulators (CCND1, CDK2) and DNA damage checkpoints factors (BLM, RAD50).

Cluster B contains mostly mitochondrial ribosomal proteins affected by AF treatment, although some (such as MRPL10) were also affected by RITA and Onc-1. Using mitochondrial membrane permeabilization assay, we found that only AF caused a small, but significant change in the mitochondrial membrane potential (**Supplementary Fig. S4C**). We also assessed mitochondrial morphology by electron microscopy but did not observe changes upon treatment (**Supplementary Fig. S4D**).

In summary, TPP data assessed by both GO and network analysis approaches revealed RNA processing as a common pathway affected by the three compounds.

RITA, AF and Onc-1 inhibit transcription in cancer cells, but not in normal cells

To investigate the effect of RITA, AF and Onc-1 on RNA processing, we visualized the incorporation of 5-ethynyluridine (EU). As shown in **Figure 4A** and **Supplementary Fig. S5A**, RITA, AF and Onc-1 completely abolished RNA synthesis, similar to known RNA Pol II inhibitors actinomycin D (ActD) and α-amanitin. Notably, the levels of total, phospho-S5 and phospho-S2 (elongating) RNA Pol II strongly decreased upon treatment in different cancer lines (**Fig. 4B** and **Supplementary Fig. S5B-C**). RNA Pol II level was rescued by the proteasome inhibitor MG132, suggesting proteasomal degradation after stalling (**Fig. 4C**). Accordingly, cycloheximide (CHX) chase experiment showed a clear decrease in RNA pol II half-life upon RITA treatment (**Fig. 4D**). Then, we investigated if the inhibition of RNA synthesis was depending on p53 activation by RITA, AF and Onc-1. RNA synthesis was also abolished in p53 KO MCF7 cells (**Supplementary Fig. S5D**).

Moreover, comparison of expression profiles upon ActD and CDK12/CDK13 inhibitor THZ531 revealed similarities with the transcriptional response to RITA, AF and Onc-1, even though different cancer cell lines were used (**Supplementary Fig. S5E-F**). We confirmed that the oncogenes involved in RITA-

induced cell death were also downregulated at protein level by THZ531 and ActD treatment (**Supplementary Fig. S5G**).

Strikingly, RITA, AF and Onc-1 did not prevent EU incorporation and RNA synthesis in normal human fibroblasts (**Fig. 4E**). In contrast, ActD and α-amanitin completely shut down transcription in non-transformed cells as well. Thus, the inhibition of transcription by RITA, AF and Onc-1 occurs selectively in cancer cells, contrary to other RNA Pol II inhibitors.

Several splicing/RNA binding factors were among the top common TPP hits, including CIRBP and RBM8A for all three compounds and SUGP1, SF3B2 and GRSF1 for any two of them. Therefore, we reasoned that RITA, AF and Onc-1 might affect RNA splicing. Indeed, all three compounds induced the formation of enlarged sc35 speckle domains (splicing factor compartments, SFCs), which were previously described upon RNA pol II or splicing inhibition (25) (**Fig. 4F** and **Supplementary Fig. S5A**).

Not only RNA Pol II but also Pol I was inhibited by the compounds, as evidenced by shuttling of the RNA helicase DDX21 from the nucleoli to the nucleoplasm (**Fig. 4G**), which is known to occur upon RNA Pol I inhibition (26). Consistently, protein level of POLR1A, the main subunit of RNA Pol I, was decreased upon treatment to the same extent as upon specific Pol I inhibitor BMH21 (**Fig. 4H**). Finally, we compared the inhibition of both Pol II and Pol I by testing the expression of RNA Pol II- and RNA Pol I-regulated RNAs, MYC mRNA and 45S pre-ribosomal RNA, respectively, upon a broad range of compounds' concentrations in MCF7 cells (**Fig. 4I**). Expression of both genes substantially decreased by the three compounds, indicating the block of both RNA polymerases. To exclude the effect of p53-mediated Myc repression (27), we used MCF7 p53KO cells and got a similar result (**Supplementary Fig. S5H**). RNA Pol I inhibition (i.e., upon low doses of ActD) and nucleolar stress activate p53 through the release of MDM2-binding protein RPL11 (28), therefore we tested if RITA had the same effect (**Supplementary Fig. S5I**). SiRNA-mediated RPL11 knock-down rescued p53 stabilization by 5nM ActD but not upon RITA, demonstrating that nucleolar stress is not involved in p53 activation upon RITA.

FACS analysis of synchronized cells using BrdU/PI staining showed that RITA-induced cell death occurs mainly in early S phase (**Supplementary Fig. S6A**), suggesting replication stress, in line with previous study (29). Thus, we addressed the question whether RNA Pol II inhibition was a consequence of replication stalling. Using cells synchronized in early G1 by lovastatin and treated with RITA before they entered S-phase, we found that the inhibition of transcription occurred in G1 and was therefore independent of replication stress. Further, we demonstrated that early S-phase arrest and replication stress (as manifested by γH2AX induction) induced by double thymidine block were not sufficient to inhibit transcription (**Supplementary Fig. S6B-C**).

To investigate the mechanism of RNA polymerase inhibition, we tested whether RITA, AF and Onc-1 can intercalate DNA by performing a thiazole orange (ThO) displacement assay. No DNA intercalation was observed at doses 12 to 60 times higher than those used in cells (**Supplementary Fig. S7A**), demonstrating that these compounds are not DNA intercalating agents. Interestingly, gene set enrichment analysis (GSEA) of our microarray data revealed an enrichment of UV response genes among the DEGs induced by all three compounds (**Supplementary Fig. S7B**). This correlates with the UV-like (30), pan-nuclear yH2AX staining, different from the discrete nuclear foci associated with DNA breaks (**Supplementary Fig. S7C**). To investigate the possibility that Pol II stalling might be caused by DNA adducts, we performed ASCC2 foci formation analysis in MCF7 cells, a marker for cell response to DNA alkylation (31). Although we indeed observed formation of ASCC2 foci (**Supplementary Fig. S7D-E**), they were induced to a lesser extent than foci formed upon low dose of alkylating agent methyl methanesulfonate (MMS).

Altogether, our data confirm the results obtained via TPP analysis and demonstrate that RITA, AF and Onc-1 inhibit RNA Pol I and Pol II-mediated transcription and interfere with RNA processing such as splicing.

RITA, AF and Onc-1 cancer-specific effects are dependent on oxidative stress

As discussed previously, RITA, AF and Onc-1 induce a strong oxidative stress (**Fig. 1F**). This was associated with oxidative DNA damage as assessed by immunostaining with 8-oxo-7,8-dihydro-2'-deoxyguanosine (8-oxodG) antibody (**Supplementary Fig. S8A**). Oxidative stress-dependent growth suppression has been previously described for all three compounds (22,32,33) and we confirmed in our cell models that two antioxidants, resveratrol and nordihydroguaiaretic acid (NDGA), rescue different cancer lines from apoptosis and growth suppression induced by RITA, AF and Onc-1 (**Fig. 5A-B** and **Supplementary Fig. S8B-C**). Notably, antioxidants also prevented RNA Pol II stalling and degradation in a p53-independent way (**Fig. 5C** and **Supplementary Fig. S8D**), as well as inhibition of pro-survival genes (**Fig. 5D-E** and **Supplementary Fig. S8E**).

As cancer cells have increased ROS levels and therefore they are more sensitive to further oxidative stress (34), we hypothesized that induction of ROS could be the reason for cancer selectivity of our compounds. To test this idea, we used a model of increased ROS upon HRasV12$^{ER\text{-}TAM}$ induction in BJ-hTert fibroblasts. We found that RITA, AF and Onc-1 suppressed the growth of fibroblasts upon HRasV12$^{ER\text{-}TAM}$ activation by tamoxifen (**Fig. 5F**) followed by the increase of the basal ROS level (**Supplementary Fig. S8F**). Moreover, we observed a significant downregulation of RNA Pol II CTD phosphorylation only upon HRas^{V12} induction (**Fig. 5G**).

Taken together, our results suggest that the cancer selectivity of transcription inhibition and growth suppression by the three compounds is dependent on oncogene-induced oxidative stress.

RITA, AF and Onc-1 inhibit homologous recombination-mediated DNA repair

It has been suggested that DNA repair factors are among the most effected genes upon inhibition of transcription elongation (4). Indeed, upon treatments the DNA repair factors CtIP, RPA32, WRAP53, RNF168, RNF8 and Rad51 (**Supplementary Fig. S9A**) were downregulated, the homologous recombination (HR)-associated protein Rad51 and its partners RNF8 and RNF168 being the most prominently decreased (**Fig. 6A** and **Supplementary Fig. S9B**). The observed decrease of these proteins

was associated with transcriptional repression (**Fig. 6B**), but not with protein stability, as measured by CHX chase experiment (**Supplementary Fig. S9C**).

We confirmed that HR was impaired upon treatment by RITA, AF and Onc-1 using U2OS cells harboring stably integrated reporter construct for HR (DR-GFP), where repair of I-SceI-induced break by HR leads to a functional GFP gene. As shown in **Figure 6C**, treatment with RITA, AF or Onc-1 leads to a stable decrease of GFP-positive cells, indicating impairment of the HR repair system.

Overexpression of Rad51, RNF8 and RNF168 did not rescue RNA Pol II inhibition or downregulation of pro-survival genes (**Fig. 6D** and **Fig. Supplementary Fig. S9D**), but we observed a partial rescue of γH2AX when overexpressing the three repair factors simultaneously, indicating that inhibition of Rad51 and its partners plays a role in the replication stress observed upon RITA (**Fig. 6D**). However, the rescue of γH2AX was not sufficient to increase cell viability (**Supplementary Fig. S9E**), highlighting the importance of the downregulation of pro-survival factors for apoptosis induction.

RITA, AF and Onc-1 sensitize to PARP inhibition

As DNA repair, and more specifically HR, is impaired due to the transcription inhibition of HR factors by RITA, AF and Onc-1, we hypothesized that these compounds could synergize with PARP inhibition to efficiently kill cancer cells. Therefore, we used sub-lethal doses of RITA, AF and Onc-1 in combination with two PARP inhibitors, olaparib (FDA-approved) and talazoparib (currently in clinical trials). Remarkably, we observed synthetic lethality with both inhibitors in MCF7 (**Fig. 6E-F** and **Supplementary Fig. S9F**) and OVCAR-3 cells (**Supplementary Fig. S9G**). We tested the combination *ex vivo* in primary ascites-derived cells from patients with high-grade serous ovarian cancer (HGS-OC) and observed similar effects (**Fig. 6G**), demonstrating the therapeutic potential of a combination of RITA, AF or Onc-1 with PARP inhibition both *in vitro* and *ex vivo*. Furthermore, we observed synthetic lethality of RITA combination with PARP inhibitors in samples derived from breast cancer patients in 3D conditions *ex vivo*. Notably, we found that the beneficial effect of this combination was evident in patient

samples with high Ki67 index and tumor grade, i.e., highly malignant tumors (**Fig. 6H**). Similarly, synthetic lethality was significantly enhanced upon activation of oncogene in cMyc-inducible U2OS cells (U2OS cMyc$^{ER\text{-}Tam}$) (**Supplementary Fig. S9H**). These findings might provide opportunities for novel therapeutic interventions in cancer.

DISCUSSION

Identification of small molecules MoA has always been a challenge in drug development. It became particularly important with the rise of personalized medicine and targeted therapies. TPP has been developed as a novel approach for the identification of small molecules targets. However, finding the correct target among the TPP hits is challenging given the number of proteins with thermal stability shifts due to secondary events. TPP is also limited to soluble proteins; additional restrictions inherent to quantitative proteomics may lead to a number of false negatives. For example, p53 and TrxR1, two previously described direct binding targets of RITA (11,23), were not found in our TPP screen. However, our study demonstrates how comprehensive analysis of the global modulation of protein interactions at the whole proteome level by TPP can help to decipher therapeutic MoA.

Our TPP analysis shows that mRNA maturation machinery is significantly affected by RITA, AF and Onc-1 treatment. Applying GO biological processes terms and a more integrated view of protein-protein interaction network revealed a striking overlap between the three treatments, with RNA processing being the common process. Validation of these findings confirmed the inhibition of RNA Pol I and Pol II-mediated transcription selectively in cancer cells. This transcription blockade leads to the loss of expression of dozens of vital oncogenes, involved in major oncogenic pathways, such as PDGF-, EGFR-, VEGF-, Insulin/IGF/MAPKK-, FGF-, Hedgehog-, TGF-beta- and PI3K signaling pathways.

Targeting transcription for anti-cancer therapy has been considered to be too toxic to normal cells. However, recent studies have challenged this view by showing that the expression of oncogenes required

for the survival of cancer cells is highly dependent on uninterrupted active transcription. For instance, blocking RNA pol II function affects more c-Myc transformed cells than their normal counterparts (35). This 'transcriptional addiction' of cancer cells creates a therapeutic window allowing selective anti-cancer growth suppression (3). Our results are in line with these ideas. We show that inhibition of transcription in cancer cells by RITA, AF and Onc-1 leads to the preferential loss of a crucial set of oncogenes and therefore target the 'Achilles' heel' of cancer cells, exerting a highly selective effects on cancer, but not normal cells.

How to achieve selectivity for tumor cells without affecting normal tissues is one of the main challenges for anticancer drug discovery. One of the cancer cells vulnerabilities is a high basal level of ROS, leading to the dependence on high expression of their antioxidant systems. Therefore, compounds increasing the oxidative stress may induce cancer cell death while sparing normal cells, which have lower ROS levels and therefore can cope with ROS increase. Indeed, it has been shown that normal cells keep a low level of ROS upon exposure to RITA (23). RITA, AF and Onc-1 all increase oxidative stress in cells and different antioxidants can prevent their cytotoxic effect (22,32,33). Moreover, head and neck cancer cells with high level of antioxidant systems are more resistant to RITA (36). Here we show that high level of intracellular ROS is important not only for apoptosis induced by RITA, AF and Onc-1 but also for their activity as RNA polymerase inhibitors. We detected oxidative DNA damage manifested as 8-oxodG upon RITA, AF and Onc-1, in line with report about AF (32). Importantly, a widespread transcriptional silencing is induced upon base excision repair (BER) of oxidative DNA damage (37). Taken together, these data suggest that the inhibition of transcription by the three compounds could be caused by BER of oxidized DNA bases. In addition, we cannot exclude the possibility that the three compounds may cause nucleotide imbalance, for instance, through oxidation of guanine, which might lead to a disruption of RNA synthesis. This hypothesis will be investigated in the future.

Overall, our data suggest that RITA, AF and Onc-1 high selectivity for cancer cells can be explained by their simultaneous targeting of multiple cancer vulnerabilities, including oncogene addiction, increased

ROS and replication stress (as summarized in **Supplementary Fig. S10**). Our study paves a way to rational treatment designs with RITA, AF and Onc-1. We found that DNA repair factors, including HR factors Rad51, RNF8 and RNF168 are strongly repressed upon RITA, AF and Onc-1, similar to CDK12/CDK13 inhibitors (4). HR deficient cells, such as BRCA2-mutant cells, are known to be particularly sensitive to PARP inhibitors (38). Thus, compounds such as RITA, AF and Onc-1, which simultaneously cause replication stress and inhibit HR, are very attractive for combination therapy with PARP inhibitors to achieve synthetic lethality in cancer cells with functional HR.

ACKNOWLEDGEMENTS

We thank all our colleagues for sharing precious reagents and material with us, especially Prof. J. Bartek (Danish Cancer Society Research Center and Karolinska Institute) and Dr. M. Farnebo (Karolinska Institute). This study was supported by the Swedish Cancer Society, the Swedish Research Council and Knut and Alice Wallenberg Foundation. SP has been supported by a fellowship from Wenner Gren Foundation.

REFERENCES

1. Schenone M, Dančík V, Wagner BK, Clemons PA. Target identification and mechanism of action in chemical biology and drug discovery. Nat Chem Biol. 2013;9:232–40.

2. Savitski MM, Reinhard FBM, Franken H, Werner T, Savitski MF, Eberhard D, et al. Tracking cancer drugs in living cells by thermal profiling of the proteome. Science. 2014;346:1255784.

3. Bradner JE, Hnisz D, Young RA. Transcriptional Addiction in Cancer. Cell. 2017;168:629–43.

4. Zhang T, Kwiatkowski N, Olson CM, Dixon-Clarke SE, Abraham BJ, Greifenberg AK, et al. Covalent targeting of remote cysteine residues to develop CDK12 and CDK13 inhibitors. Nat Chem Biol. 2016;12:876–84.

5. Pagliarini R, Shao W, Sellers WR. Oncogene addiction: pathways of therapeutic response, resistance, and road maps toward a cure. EMBO Rep. 16:280–96.

6. Reinhold WC, Sunshine M, Liu H, Varma S, Kohn KW, Morris J, et al. CellMiner: a web-based suite of genomic and pharmacologic tools to explore transcript and drug patterns in the NCI-60 cell line set. Cancer Res. 2012;72:3499–511.

7. Franken H, Mathieson T, Childs D, Sweetman GMA, Werner T, Tögel I, et al. Thermal proteome profiling for unbiased identification of direct and indirect drug targets using multiplexed quantitative mass spectrometry. Nat Protoc. 2015;10:1567–93.

8. Mi H, Huang X, Muruganujan A, Tang H, Mills C, Kang D, et al. PANTHER version 11: expanded annotation data from Gene Ontology and Reactome pathways, and data analysis tool enhancements. Nucleic Acids Res. 2017;45:D183–9.

9. Szklarczyk D, Franceschini A, Wyder S, Forslund K, Heller D, Huerta-Cepas J, et al. STRING v10: protein-protein interaction networks, integrated over the tree of life. Nucleic Acids Res. 2015;43:D447-452.

10. Pierce AJ, Johnson RD, Thompson LH, Jasin M. XRCC3 promotes homology-directed repair of DNA damage in mammalian cells. Genes Dev. 1999;13:2633–8.

11. Issaeva N, Bozko P, Enge M, Protopopova M, Verhoef LGGC, Masucci M, et al. Small molecule RITA binds to p53, blocks p53-HDM-2 interaction and activates p53 function in tumors. Nat Med. 2004;10:1321–8.

12. Grinkevich VV, Nikulenkov F, Shi Y, Enge M, Bao W, Maljukova A, et al. Ablation of Key Oncogenic Pathways by RITA-Reactivated p53 Is Required for Efficient Apoptosis. Cancer Cell. 2009;15:441–53.

13. Wanzel M, Vischedyk JB, Gittler MP, Gremke N, Seiz JR, Hefter M, et al. CRISPR-Cas9-based target validation for p53-reactivating model compounds. Nat Chem Biol. 2016;12:22–8.

14. Saei AA, Beusch CM, Chernobrovkin A, Sabatier P, Zhang B, Tokat ÜG, et al. ProTargetMiner as a proteome signature library of anticancer molecules for functional discovery. Nat Commun. 2019;10:1–13.

15. Akama T, Shida Y, Sugaya T, Ishida H, Gomi K, Kasai M. Novel 5-aminoflavone derivatives as specific antitumor agents in breast cancer. J Med Chem. 1996;39:3461–9.

16. Meng L, Kohlhagen G, Liao Z, Antony S, Sausville E, Pommier Y. DNA-protein cross-links and replication-dependent histone H2AX phosphorylation induced by aminoflavone (NSC 686288), a novel anticancer agent active against human breast cancer cells. Cancer Res. 2005;65:5337–43.

17. Guo W, Wu S, Liu J, Fang B. Identification of a small molecule with synthetic lethality for K-ras and protein kinase C iota. Cancer Res. 2008;68:7403–8.

18. Wu S, Wang L, Guo W, Liu X, Liu J, Wei X, et al. Analogues and derivatives of Oncrasin-1, a Novel Inhibitor of the C-Terminal Domain of RNA Polymerase II, and Their Antitumor Activities. J Med Chem. 2011;54:2668–79.

19. Guo W, Wu S, Wang L, Wei X, Liu X, Wang J, et al. Antitumor activity of a novel oncrasin analogue is mediated by JNK activation and STAT3 inhibition. PloS One. 2011;6:e28487.

20. Guo W, Wu S, Wang L, Wang R, Wei X, Liu J, et al. Interruption of RNA processing machinery by a small compound 1-[(4-chlorophenyl) methyl]-1H-indole-3-carboxaldehyde (oncrasin-1). Mol Cancer Ther. 2009;8:441–8.

21. McLean LS, Brantley E. Apoptotic mechanism of novel anticancer agents is mediated by MAPKs in breast cancer cells. FASEB J. 2013;27:1105.3-1105.3.

22. Shi Y, Nikulenkov F, Zawacka-Pankau J, Li H, Gabdoulline R, Xu J, et al. ROS-dependent activation of JNK converts p53 into an efficient inhibitor of oncogenes leading to robust apoptosis. Cell Death Differ. 2014;21:612–23.

23. Hedström E, Eriksson S, Zawacka-Pankau J, Arnér ESJ, Selivanova G. p53-dependent inhibition of TrxR1 contributes to the tumor-specific induction of apoptosis by RITA. Cell Cycle Georget Tex. 2009;8:3584–91.

24. Enge M, Bao W, Hedström E, Jackson SP, Moumen A, Selivanova G. MDM2-dependent downregulation of p21 and hnRNP K provides a switch between apoptosis and growth arrest induced by pharmacologically activated p53. Cancer Cell. 2009;15:171–83.

25. Girard C, Will CL, Peng J, Makarov EM, Kastner B, Lemm I, et al. Post-transcriptional spliceosomes are retained in nuclear speckles until splicing completion. Nat Commun. 2012;3:994.

26. Calo E, Gu B, Bowen ME, Aryan F, Zalc A, Liang J, et al. Tissue–selective effects of nucleolar stress and rDNA damage in developmental disorders. Nature. 2018;554:112–7.

27. Ho JSL, Ma W, Mao DYL, Benchimol S. p53-Dependent transcriptional repression of c-myc is required for G1 cell cycle arrest. Mol Cell Biol. 2005;25:7423–31.

28. Fumagalli S, Di Cara A, Neb-Gulati A, Natt F, Schwemberger S, Hall J, et al. Absence of nucleolar disruption after impairment of 40S ribosome biogenesis reveals an rpL11-translation-dependent mechanism of p53 induction. Nat Cell Biol. 2009;11:501–8.

29. Ahmed A, Yang J, Maya-Mendoza A, Jackson DA, Ashcroft M. Pharmacological activation of a novel p53-dependent S-phase checkpoint involving CHK-1. Cell Death Dis. 2011;2:e160.

30. de Feraudy S, Revet I, Bezrookove V, Feeney L, Cleaver JE. A minority of foci or pan-nuclear apoptotic staining of γH2AX in the S phase after UV damage contain DNA double-strand breaks. Proc Natl Acad Sci U S A. 2010;107:6870–5.

31. Brickner JR, Soll JM, Lombardi PM, Vågbø CB, Mudge MC, Oyeniran C, et al. A ubiquitin-dependent signalling axis specific for ALKBH-mediated DNA dealkylation repair. Nature. 2017;551:389–93.

32. McLean L, Soto U, Agama K, Francis J, Jimenez R, Pommier Y, et al. Aminoflavone induces oxidative DNA damage and reactive oxidative species-mediated apoptosis in breast cancer cells. Int J Cancer J Int Cancer. 2008;122:1665–74.

33. Wei X, Guo W, Wu S, Wang L, Huang P, Liu J, et al. Oxidative stress in NSC-741909-induced apoptosis of cancer cells. J Transl Med. 2010;8:37.

34. Gorrini C, Harris IS, Mak TW. Modulation of oxidative stress as an anticancer strategy. Nat Rev Drug Discov. 2013;12:931–47.

35. Koumenis C, Giaccia A. Transformed cells require continuous activity of RNA polymerase II to resist oncogene-induced apoptosis. Mol Cell Biol. 1997;17:7306–16.

36. Shin D, Kim EH, Lee J, Roh J-L. RITA plus 3-MA overcomes chemoresistance of head and neck cancer cells via dual inhibition of autophagy and antioxidant systems. Redox Biol. 2017;13:219–27.

37. Allgayer J, Kitsera N, Bartelt S, Epe B, Khobta A. Widespread transcriptional gene inactivation initiated by a repair intermediate of 8-oxoguanine. Nucleic Acids Res. 2016;44:7267–80.

38. Bryant HE, Schultz N, Thomas HD, Parker KM, Flower D, Lopez E, et al. Specific killing of BRCA2-deficient tumours with inhibitors of poly(ADP-ribose) polymerase. Nature. 2005;434:913–7.

FIGURE LEGENDS

Figure 1. AF and Onc-1 phenocopy the effects of RITA in cancer cells. A, Unsupervised clustering of proteome profiles induced in lung carcinoma A549 cells by a panel of 20 anti-cancer compounds, including RITA. **B,** Chemical structures of RITA, AF and Onc-1. **C,** Correlation of sensitivity (GI50) between RITA and AF (left panel) and between RITA and Onc-1 (right panel) in the NCI-60 cell lines panel. **D,** Cell viability of cancer cells (in red) or normal immortalized cells (in grey) upon treatment by RITA, AF or Onc-1. **E,** PARP cleavage (indicating apoptosis induction), γH2AX (induction of DNA damage response), phospho-JNK and phospho-c-JUN protein levels in MCF7 cells treated with RITA, AF or Onc-1. **F,** Induction of ROS by RITA, AF or Onc-1 in MCF7 measured by DCF-DA.

Figure 2. RITA, AF and Onc-1 repress the transcription of oncogenes. A, Downregulation of selected oncogenes upon treatment by RITA, AF or Onc-1 detected by Western blot. **B,** mRNA level of p53 target genes (PUMA, NOXA, p21) and RITA-repressed oncogenes after treatment with RITA, AF or Onc-1 measured by qPCR. **C,** Heatmap of common DEGs ($p \leq 0.05$) in MCF7 cells upon treatment with RITA, AF or Onc-1, as assessed by microarray analysis. **D,** Overlap between DEGs, up-, and down-regulated genes upon the three compounds. **E,** Enrichment of oncogenes among repressed genes upon RITA, AF and Onc-1 in MCF7 cells. Significance is calculated by using Fisher's exact test. **F,** GO analysis of oncogenic pathways downregulated upon treatments with RITA, AF and Onc-1. Shown are significantly affected pathways (adjusted *p*-value <0.01) **G,** Heatmap of common differentially expressed oncogenes ($p \leq 0.05$) upon treatment with the three compounds.

Figure 3. Thermal proteome profiling (TPP) identifies RNA processing as the common target of RITA, AF and Onc-1. A, Volcano plots show all thermal shifts detected by TPP upon treatment. TPP hits (red) were defined as proteins with thermal stability shift $|\Delta T_m|>0.5$ °C between the treatment and the control in both replicates, with a *p*-value <0.05. Proteins involved in RNA processing are indicated, and

common hits upon at least two treatments are highlighted. **B,** Overlap of TPP hits upon treatment by RITA, AF and Onc-1. **C,** GO biological process terms significantly enriched (adjusted *p*-value <00.1) in TPP hits upon treatment with RITA, AF and Onc-1. The percentage indicates the number of hits relative to the GO group size. **D,** Overlap of GO biological process terms significantly enriched in TPP hits upon treatment with RITA, AF and Onc-1. **E,** STRING network analysis of the combination of TPP hits from the 3 compounds. Each ball represents a protein with significantly altered thermal stability upon at least one of the compounds. Only proteins with connections in the network are displayed. The three main clusters of protein interactions in the network identified by unbiased K-means are indicated in different colors. **F,** Relative proportion of TPP hits in A, B and C clusters affected by RITA, AF or Onc-1. **G,** Top five GO biological process terms significantly enriched in TPP hits in each cluster. The percentage indicates the number of hits relative to the GO group size.

Figure 4. RITA, AF and Onc-1 inhibit transcription by RNA Pol I and RNA Pol II. A, RNA synthesis monitored by EU incorporation in MCF7 cells treated with RITA, AF, Onc-1, ActD (2.5 μM) or α-amanitin (10 μM), then incubated 1h with 1 mM EU. EU was labelled by click chemistry and visualized by fluorescent microscopy. **B,** Total and phospho-Ser2 RNA Pol II CTD protein levels in MCF7 cells treated with RITA, AF or Onc-1. Lower panel: densitometric quantification of the bands normalized to β-actin. **C,** RNA pol II CTD protein level in MCF7 cells pretreated with 20 μM MG132 for 2h and then treated with RITA, AF or Onc-1 for 24h. **D,** CHX chase analysis of RNA pol II degradation. Upper panel: RNA pol II level in CHX-treated (10 μM) MCF7 cells upon RITA treatment. Lower panel: densitometric quantification of the bands normalized to β-actin. **E,** RNA synthesis of immortalized BJ-hTert fibroblasts treated with RITA, AF, Onc-1, ActD (2.5 μM) or α-amanitin (10 μM) for 24h analyzed as in (A). **F,** Modifications of splicing factor compartments (SFCs) detected by sc35 immunostaining in MCF7 cells treated with RITA, AF or Onc-1. **G,** DDX21 subcellular localization detected by immunofluorescence. **H**, POLR1A level in MCF7 upon 24h treatment with BMH21 (0.5 μM), RITA, AF or Onc-1. Lower panel:

densitometric quantification of POLR1A bands normalized to β-actin from two independent experiments (* $p<0.05$). **I,** 45S pre-rRNA or MYC mRNA detected by qPCR in MCF7 cells upon RITA, AF or Onc-1 (8h). RNA level (ΔCt) is relative to untreated control, RPL13A is used as housekeeping gene.

Figure 5. RITA, AF and Onc-1 effects are oxidative stress-dependent. A, Induction of apoptosis (PARP cleavage) and DNA damage response (γH2AX) in MCF7 cells treated with RITA, AF or Onc-1 for 24h in presence of antioxidants resveratrol (1 μM) or NDGA (10 μM). **B,** Cell viability of MCF7 cells treated with RITA, AF or Onc-1 for 24h in presence of resveratrol or NDGA. **C,** RNA Pol II CTD total and phospho-Ser2 levels in MCF7 cells treated with RITA, AF or Onc-1 for 24h in presence of resveratrol. **D,** Protein levels of selected RITA-downregulated oncogenes and pro-survival factors in MCF7 cells treated with RITA, AF or Onc-1 for 24h in presence of resveratrol or NDGA. **E,** mRNA level of p53 target genes and RITA-downregulated oncogenes in MCF7 cells upon RITA, AF or Onc-1 in presence of resveratrol. **F,** Cell viability of normal immortalized fibroblasts with inducible Ras system (BJ-hTert HRasV12$^{ER\text{-}Tam}$) upon 4 days of RITA, AF or Onc-1 treatment in the absence or presence of activated Ras. **G,** Total and phospho-Ser2 RNA Pol II CTD protein levels in BJ-hTert HRasV12$^{ER\text{-}Tam}$ cells upon 4 days of RITA, AF or Onc-1 treatment in the absence or presence of activated Ras. Lower panel: densitometric quantification of RNA Pol II bands normalized to β-actin, from two independent experiments (* $p<0.05$, *** $p<0.01$).

Figure 6. RITA, AF and Onc-1 inhibit homologous recombination and sensitize to PARP inhibition. A, Western blots for DNA repair factors RNF8, RNF168 and RAD51 in MCF7 cells upon RITA, AF or Onc-1 treatment. **B,** qPCR for mRNA level of DNA repair factors RNF8, RNF168 and RAD51 after treatment of MCF7 cells with RITA or AF for 8h, or with Onc-1 for 16h. **C,** HR efficiency upon treatment with RITA, AF or Onc-1 monitored using HR-reporter U2OS (DR-GFP) cells. **D,** Total and phospho-Ser2RNA pol II protein levels in MCF7 transiently overexpressing RAD51-GFP, RNF8-HA and RNF168-GFP treated with RITA for 16h. Lower panel: densitometric quantification of γH2AX bands normalized to

β-actin from two independent experiments (* $p<0.05$). **E-F,** Synthetic lethality in MCF7 cells treated with sub-lethal doses of RITA, AF or Onc-1 in presence of PARP inhibitor olaparib (E) or talazoparib (F), as assessed by crystal violet staining. Relative quantification is indicated below the pictures. **G,** Cell viability of primary ascites-derived cells from patients with high-grade serous ovarian cancer (HGS-OC), treated with RITA (0.05 μM), AF (1 μM) or Onc-1 (1 μM) for 48h in presence of olaparib 1 μM (patient 1) or 0.1 μM (patient 2) (n=3, * $p<0.05$, *** $p<0.01$). **H,** Cell viability of patient-derived primary breast cancer cells treated with sub-lethal dose of RITA in presence of olaparib or talazoparib (n=3, * $p<0.05$, *** $p<0.01$). Diagram (lower right panel) shows the correlation between the Ki67 index/tumor grade and the sensitivity to the combination of RITA with PARP inhibitors.

Figure 1.

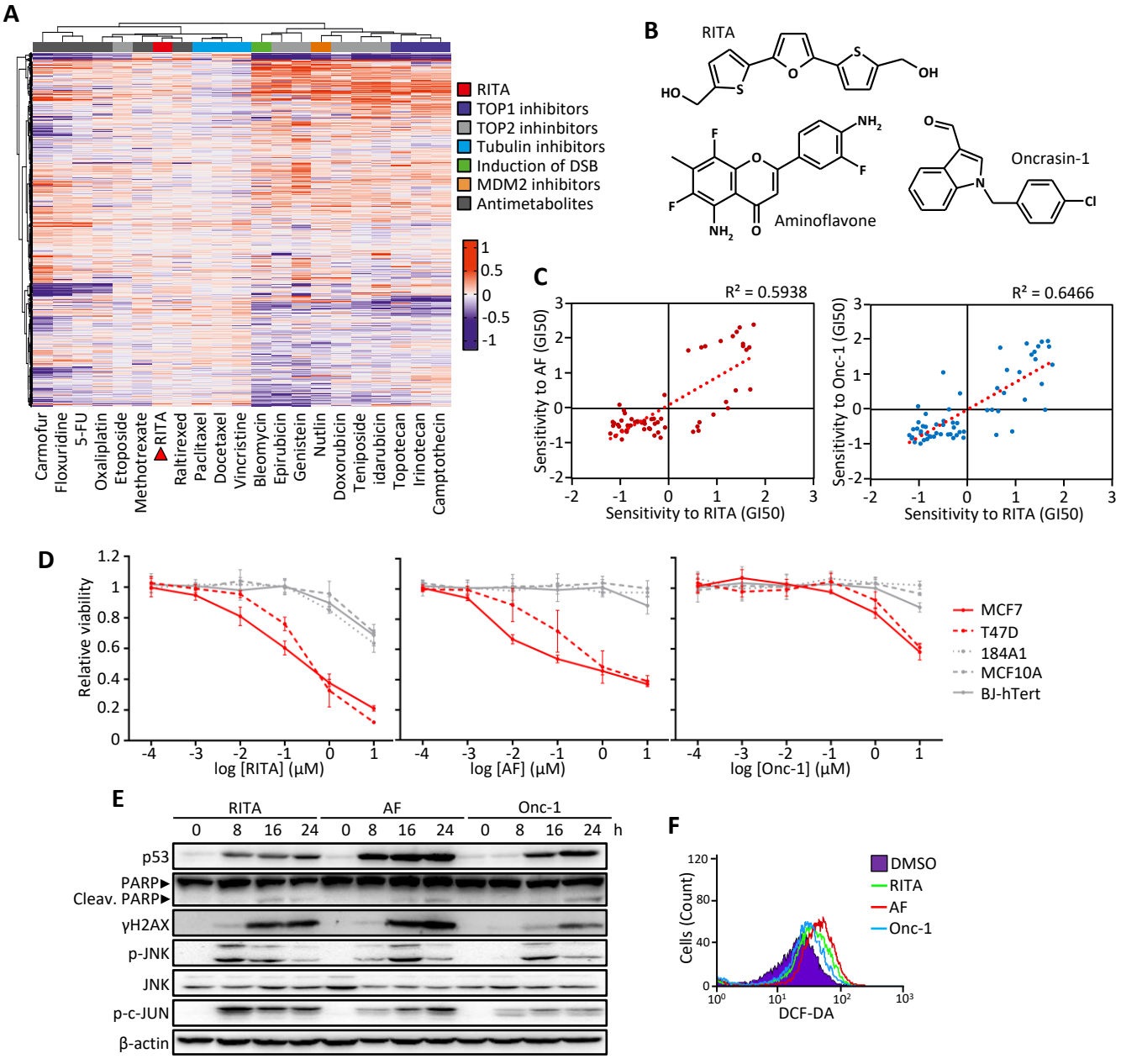
A
RITA
TOP1 inhibitors
TOP2 inhinbitors
Tubulin inhibitors
Induction of DSB
MDM2 inhibitors
Antimetabolites
1
0.5
0
-0.5
-1
Carmofur
Floxuridine
5-FU
Oxaliplatin
Etoposide
Methotrexate
RITA
Raltirexed
Paclitaxel
Docetaxel
Vincristine
Bleomycin
Epirubicin
Genistein
Nutlin
Doxorubicin
Teniposide
idarubicin
Topotecan
Irinotecan
Camptothecin
B
RITA
HO
OH
Aminoflavone
Oncrasin-1
Cl
C
R² = 0.5938
Sensitivity to AF (GI50)
Sensitivity to RITA (GI50)
R² = 0.6466
Sensitivity to Onc-1 (GI50)
Sensitivity to RITA (GI50)
D
Relative viability
log [RITA] (μM)
log [AF] (μM)
log [Onc-1] (μM)
MCF7
T47D
184A1
MCF10A
BJ-hTert
E
RITA
AF
Onc-1
0 8 16 24 0 8 16 24 0 8 16 24 h
p53
PARP▶
Cleav. PARP▶
γH2AX
p-JNK
JNK
p-c-JUN
β-actin
F
Cells (Count)
DCF-DA
DMSO
RITA
AF
Onc-1

Figure 2.

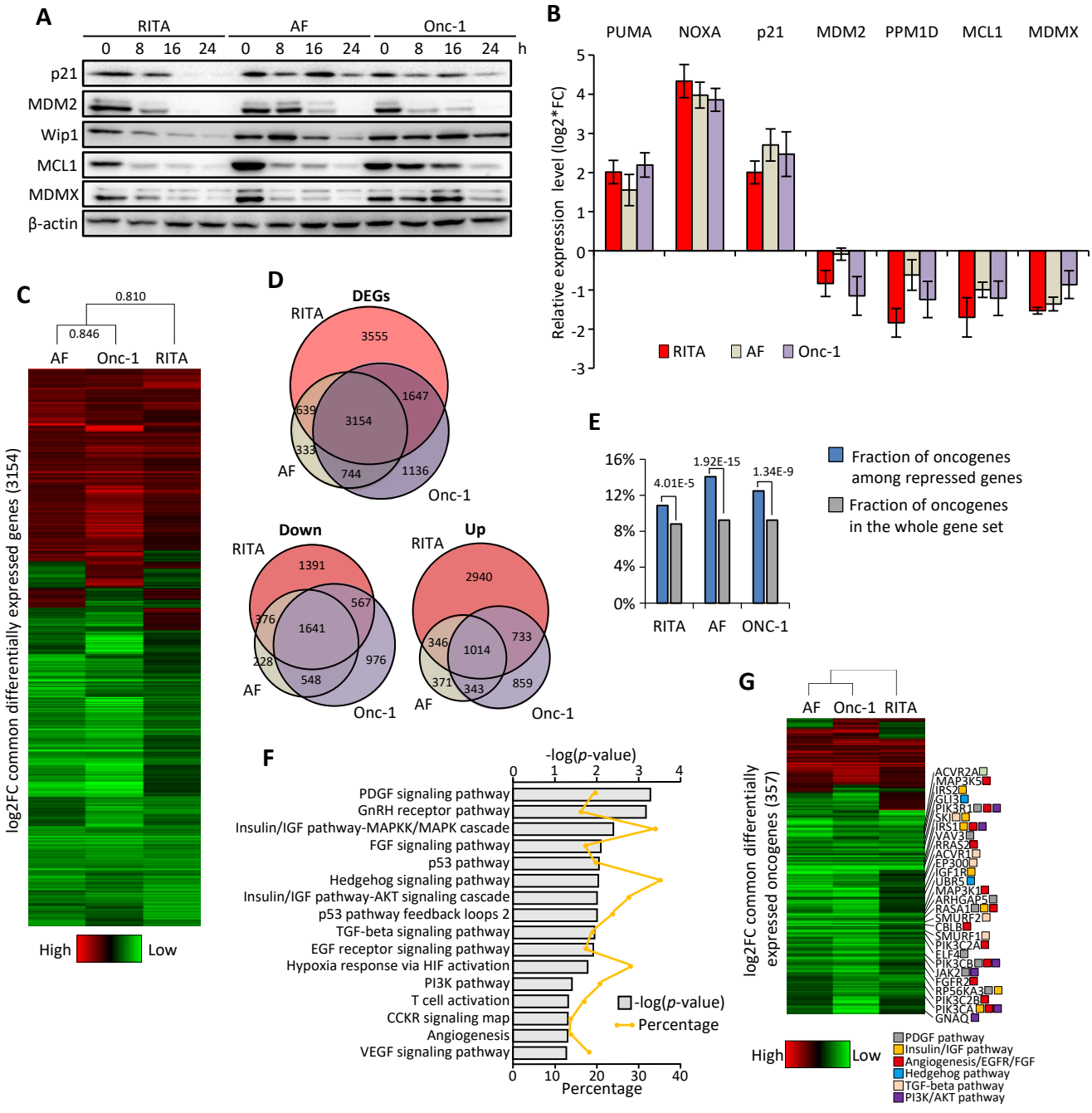
A
RITA
AF
Onc-1
0 8 16 24 0 8 16 24 0 8 16 24 h
p21
MDM2
Wip1
MCL1
MDMX
β-actin
B
PUMA NOXA p21 MDM2 PPM1D MCL1 MDMX
Relative expression level (log2*FC)
RITA AF Onc-1
C
0.810
0.846
AF Onc-1 RITA
log2FC common differentially expressed genes (3154)
High Low
D
DEGs
RITA
3555
1647
639
3154
333
744
1136
AF
Onc-1
Down
RITA
1391
567
376
1641
228
976
548
AF
Onc-1
Up
RITA
2940
733
346
1014
371
343
859
AF
Onc-1
E
16%
12%
8%
4%
0%
4.01E-5
1.92E-15
1.34E-9
RITA AF ONC-1
Fraction of oncogenes among repressed genes
Fraction of oncogenes in the whole gene set
F
-log(p-value)
0 1 2 3 4
PDGF signaling pathway
GnRH receptor pathway
Insulin/IGF pathway-MAPKK/MAPK cascade
FGF signaling pathway
p53 pathway
Hedgehog signaling pathway
Insulin/IGF pathway-AKT signaling cascade
p53 pathway feedback loops 2
TGF-beta signaling pathway
EGF receptor signaling pathway
Hypoxia response via HIF activation
PI3K pathway
T cell activation
CCKR signaling map
Angiogenesis
VEGF signaling pathway
-log(p-value)
Percentage
0 10 20 30 40
Percentage
G
AF Onc-1 RITA
log2FC common differentially expressed oncogenes (357)
ACVR2A
MAP3K5
IRS2
GLI3
PIK3R1
SKI
IRS1
VAV3
RRAS2
ACVR1
EP300
IGF1R
UBR5
MAP3K1
ARHGAP5
RASA1
SMURF2
CBLB
SMURF1
PIK3C2A
ELF4
PIK3CB
JAK2
FGFR2
RPS6KA3
PIK3C2B
PIK3CA
GNAQ
High Low
PDGF pathway
Insulin/IGF pathway
Angiogenesis/EGFR/FGF
Hedgehog pathway
TGF-beta pathway
PI3K/AKT pathway

Figure 3.

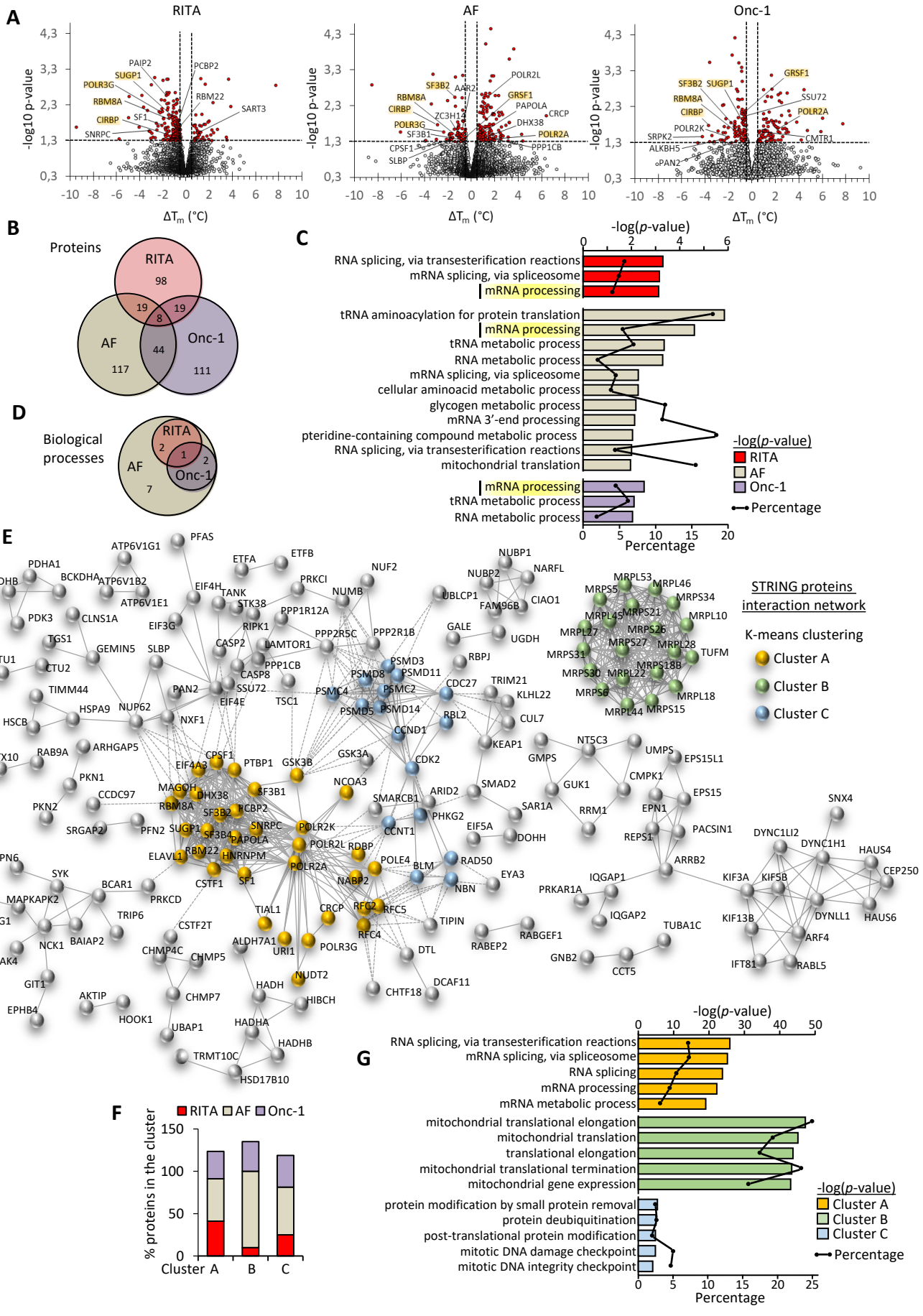
A
RITA
AF
Onc-1
-log10 p-value
ΔTm (°C)
PAIP2
PCBP2
SUGP1
POLR3G
RBM8A
RBM22
SART3
CIRBP
SF1
SNRPC
SF3B2
AAR2
POLR2L
GRSF1
PAPOLA
CRCP
ZC3H14
DHX38
SF3B1
POLR2A
CPSF1
PPP1CB
SLBP
SF3B2
SUGP1
GRSF1
RBM8A
SSU72
CIRBP
POLR2A
POLR2K
SRPK2
CMTR1
ALKBH5
PAN2
B
Proteins
RITA
98
19
19
8
AF
117
44
Onc-1
111
C
-log(p-value)
RNA splicing, via transesterification reactions
mRNA splicing, via spliceosome
mRNA processing
tRNA aminoacylation for protein translation
mRNA processing
tRNA metabolic process
RNA metabolic process
mRNA splicing, via spliceosome
cellular aminoacid metabolic process
glycogen metabolic process
mRNA 3′-end processing
pteridine-containing compound metabolic process
RNA splicing, via transesterification reactions
mitochondrial translation
mRNA processing
tRNA metabolic process
RNA metabolic process
-log(p-value)
RITA
AF
Onc-1
Percentage
Percentage
D
Biological processes
RITA
2
1
2
AF
7
Onc-1
E
STRING proteins interaction network
K-means clustering
Cluster A
Cluster B
Cluster C
F
RITA AF Onc-1
% proteins in the cluster
Cluster A
B
C
G
-log(p-value)
RNA splicing, via transesterification reactions
mRNA splicing, via spliceosome
RNA splicing
mRNA processing
mRNA metabolic process
mitochondrial translational elongation
mitochondrial translation
translational elongation
mitochondrial translational termination
mitochondrial gene expression
protein modification by small protein removal
protein deubiquitination
post-translational protein modification
mitotic DNA damage checkpoint
mitotic DNA integrity checkpoint
-log(p-value)
Cluster A
Cluster B
Cluster C
Percentage
Percentage

Figure 4.

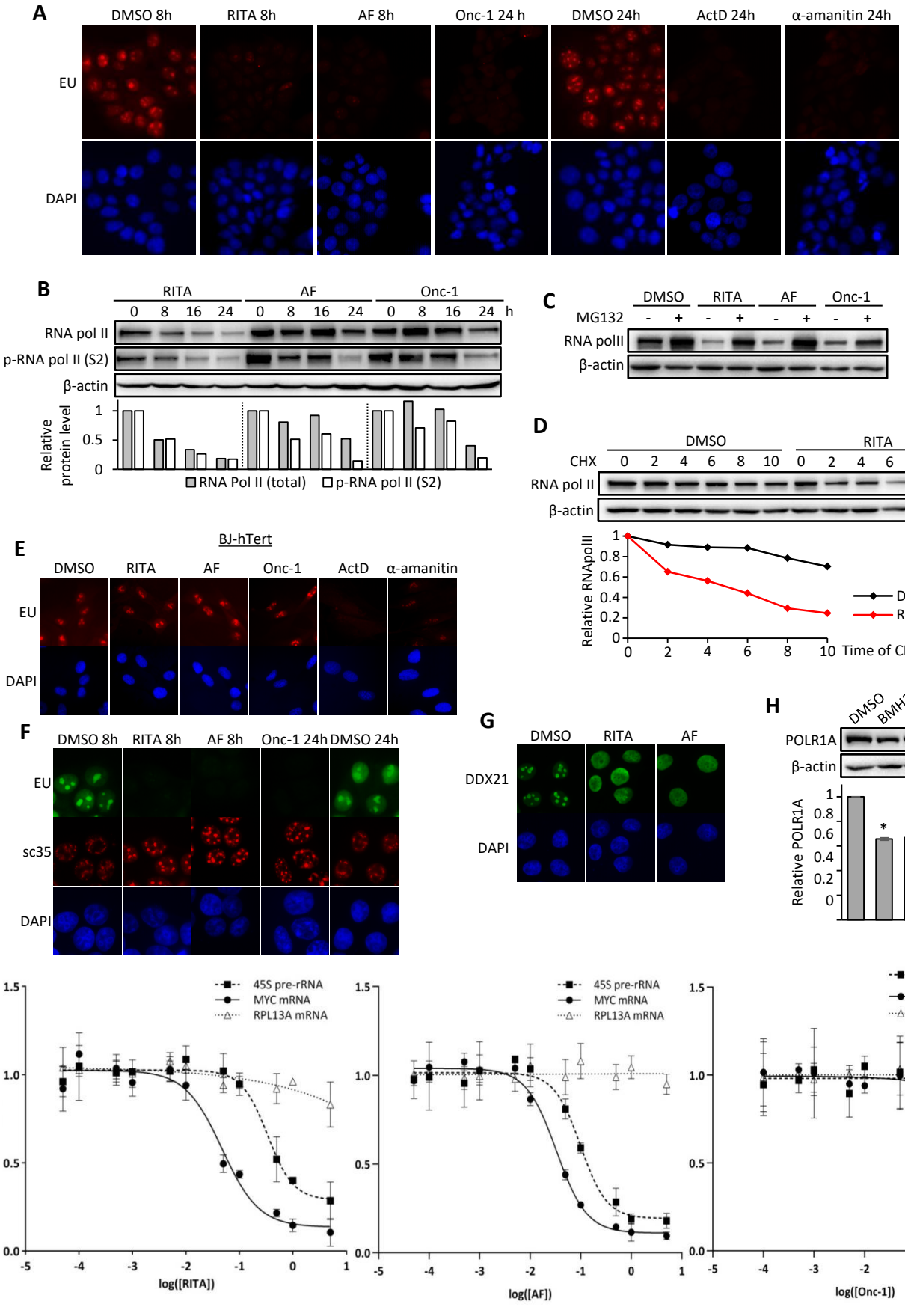
A
DMSO 8h
RITA 8h
AF 8h
Onc-1 24 h
DMSO 24h
ActD 24h
α-amanitin 24h
EU
DAPI
B
RITA
AF
Onc-1
0 8 16 24 0 8 16 24 0 8 16 24 h
RNA pol II
p-RNA pol II (S2)
β-actin
Relative protein level
1
0.5
0
RNA Pol II (total)
p-RNA pol II (S2)
C
DMSO
RITA
AF
Onc-1
MG132 - + - + - + - +
RNA polII
β-actin
D
DMSO
RITA
CHX 0 2 4 6 8 10 0 2 4 6 8 10 h
RNA pol II
β-actin
Relative RNApolII
1
0.8
0.6
0.4
0.2
0
0 2 4 6 8 10
Time of CHX (h)
DMSO
RITA
E
BJ-hTert
DMSO
RITA
AF
Onc-1
ActD
α-amanitin
EU
DAPI
F
DMSO 8h
RITA 8h
AF 8h
Onc-1 24h
DMSO 24h
EU
sc35
DAPI
G
DMSO
RITA
AF
DDX21
DAPI
H
DMSO
BMH21
RITA
AF
Onc-1
POLR1A
β-actin
Relative POLR1A
1
0.8
0.6
0.4
0.2
0
*
I
45S pre-rRNA
MYC mRNA
RPL13A mRNA
Relative RNA level
1.5
1.0
0.5
0.0
-5 -4 -3 -2 -1 0 1
log([RITA])
log([AF])
log([Onc-1])

Figure 5.

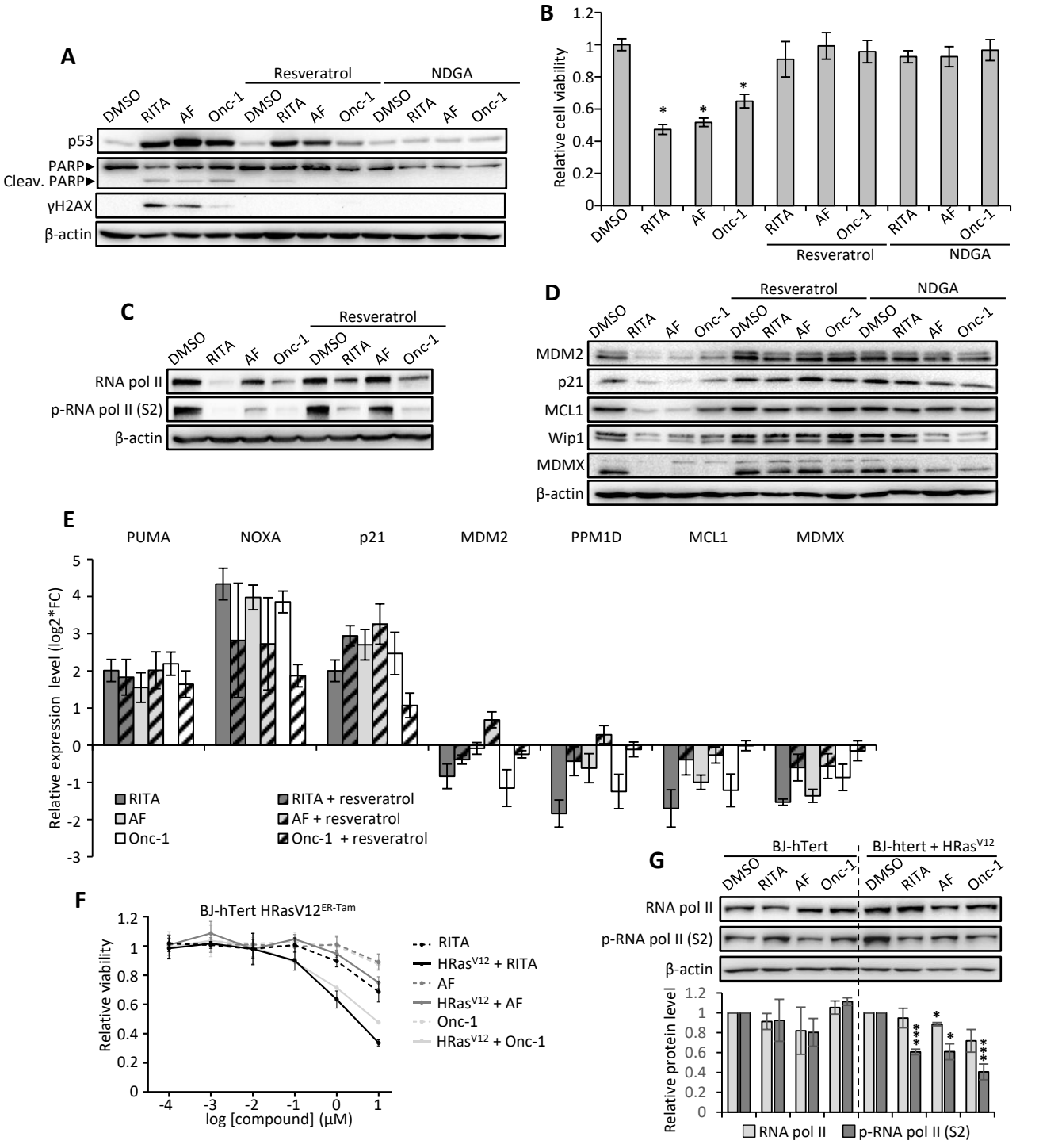
A
Resveratrol
NDGA
DMSO
RITA
AF
Onc-1
p53
PARP▶
Cleav. PARP▶
γH2AX
β-actin
B
Relative cell viability
Resveratrol
NDGA
C
RNA pol II
p-RNA pol II (S2)
β-actin
D
MDM2
p21
MCL1
Wip1
MDMX
β-actin
E
PUMA
NOXA
p21
MDM2
PPM1D
MCL1
MDMX
Relative expression level (log2*FC)
RITA
AF
Onc-1
RITA + resveratrol
AF + resveratrol
Onc-1 + resveratrol
F
BJ-hTert HRasV12ER-Tam
Relative viability
log [compound] (μM)
RITA
HRasV12 + RITA
AF
HRasV12 + AF
Onc-1
HRasV12 + Onc-1
G
BJ-hTert
BJ-htert + HRasV12
RNA pol II
p-RNA pol II (S2)
β-actin
Relative protein level

Figure 6.

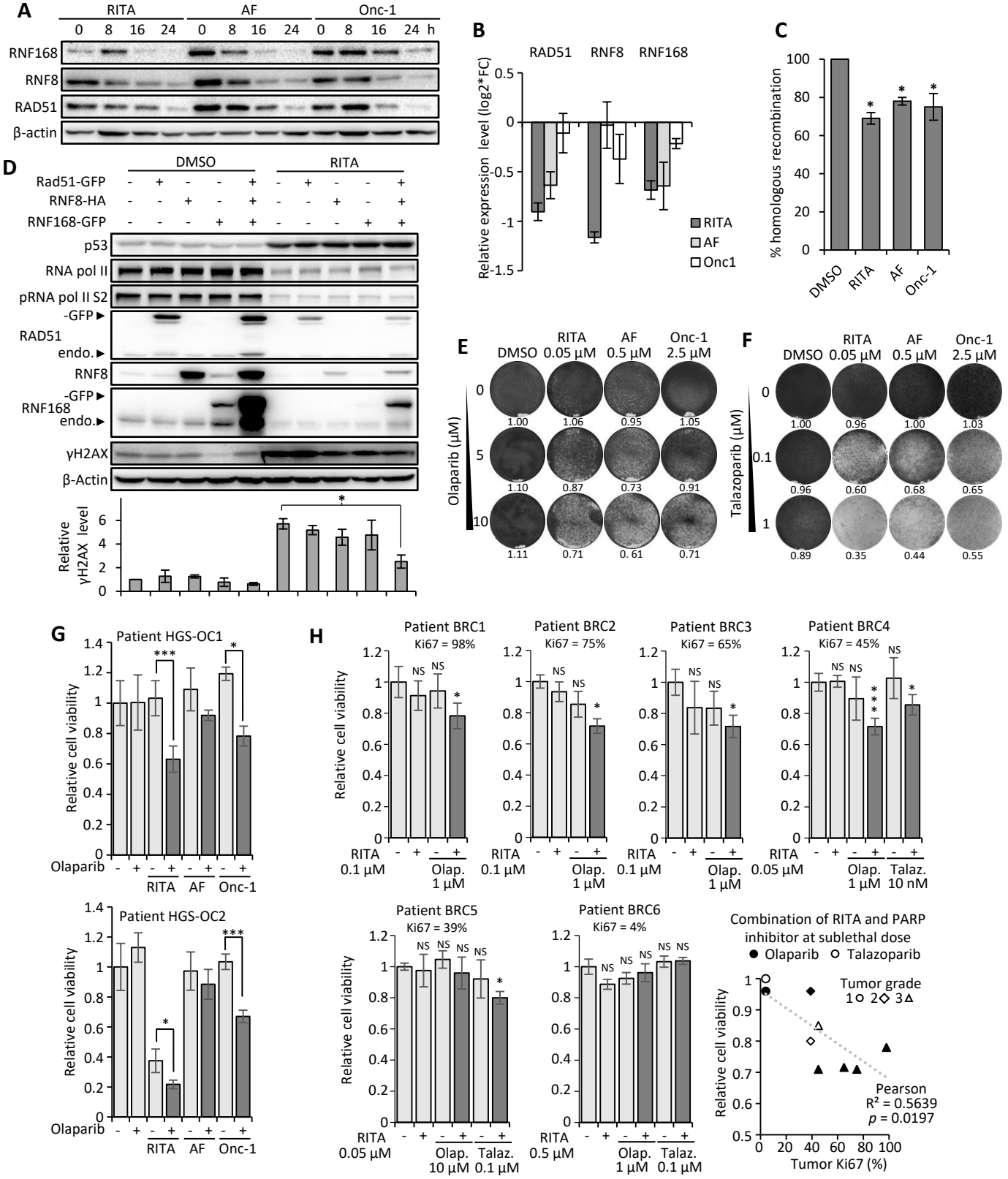
A
RITA
AF
Onc-1
0 8 16 24 0 8 16 24 0 8 16 24 h
RNF168
RNF8
RAD51
β-actin
B
RAD51 RNF8 RNF168
Relative expression level (log2*FC)
RITA
AF
Onc1
C
% homologous recombination
DMSO
RITA
AF
Onc-1
D
DMSO
RITA
Rad51-GFP
RNF8-HA
RNF168-GFP
p53
RNA pol II
pRNA pol II S2
-GFP ▶
RAD51
endo.▶
RNF8
-GFP ▶
RNF168
endo.▶
γH2AX
β-Actin
Relative γH2AX level
E
DMSO
RITA 0.05 μM
AF 0.5 μM
Onc-1 2.5 μM
Olaparib (μM)
1.00 1.06 0.95 1.05
1.10 0.87 0.73 0.91
1.11 0.71 0. 61 0.71
F
DMSO
RITA 0.05 μM
AF 0.5 μM
Onc-1 2.5 μM
Talazoparib (μM)
1.00 0.96 1.00 1.03
0.96 0.60 0.68 0.65
0.89 0.35 0.44 0.55
G
Patient HGS-OC1
Relative cell viability
Olaparib
RITA AF Onc-1
Patient HGS-OC2
H
Patient BRC1
Ki67 = 98%
Patient BRC2
Ki67 = 75%
Patient BRC3
Ki67 = 65%
Patient BRC4
Ki67 = 45%
RITA 0.1 μM
Olap. 1 μM
RITA 0.05 μM
Olap. 1 μM Talaz. 10 nM
Patient BRC5
Ki67 = 39%
Patient BRC6
Ki67 = 4%
RITA 0.05 μM
Olap. 10 μM Talaz. 0.1 μM
RITA 0.5 μM
Olap. 1 μM Talaz. 0.1 μM
Combination of RITA and PARP inhibitor at sublethal dose
Olaparib
Talazoparib
Tumor grade 1 2 3
Relative cell viability
Pearson
R² = 0.5639
p = 0.0197
Tumor Ki67 (%)